Supplementary Information

A fluid-to-solid jamming transition underlies vertebrate body axis elongation

A. Mongera, P. Rowghanian, H.J. Gustafson, E. Shelton, D.A. Kealhofer, E.K. Carn, F. Serwane, A.A. Lucio, J. Giammona & O. Campàs

Supplementary Figure 1

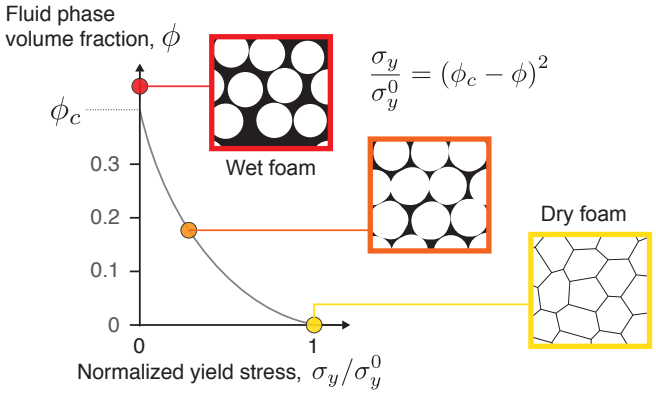

Figure S1: **Yield stress in aqueous foams.** Theoretical dependence of the yield stress σ_y on the volume fraction ϕ of fluid between bubbles in aqueous foams[1]. The yield stress is maximal for dry foams ($\phi = 0$) and vanishes at a critical value ϕ_c (wet foam).

Supplementary Figure 2

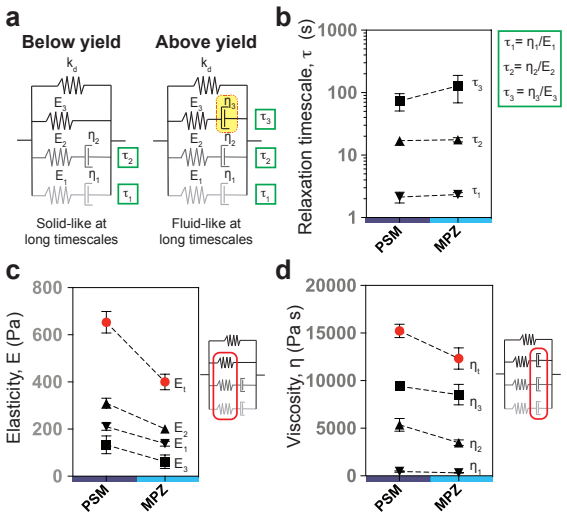

Figure S2: **Quantification of tissue viscoelastic properties and relaxation timescales below and above the yield stress in both PSM and MPZ. a**, 1D rheological diagrams capturing the mechanical response of the analyzed tissues. Below yield, the tissue is characterized by two relaxation timescales (τ_1 and τ_2), associated to two Maxwell-like components acting in parallel (with elastic elements E_1 and E_2 and viscous elements η_1 and η_2), and an elastic component (E_3) that characterizes the tissue elasticity at small applied strains. At long timescales, the tissue behaves like an elastic solid below yield. Above yield, the tissue behaves like a fluid at long timescales and is characterized by an additional viscous element (η_3) and relaxation timescale (τ_3). The elastic element k_d effectively accounts for the droplet restoring force associated to its interfacial tension (capillary stress), as previously described[20]. **b**, Measured stress relaxation timescales in PSM and MPZ. **c**, All elastic components, including the tissue-scale elasticity (E_3), are larger in the PSM than in the MPZ. The total elastic modulus of the tissue at short timescales is plotted in red. **d**, The viscous components also display larger values in the PSM than in the MPZ. The total viscosity of the tissue at long timescales above yield is plotted in red. For PSM, n=26 for measurements of τ_1, τ_2, E_1, E_2, η_1, η_2 and n=15 for measurements of τ_3, E_3 and η_3. For MPZ, n=49 for measurements of τ_1, τ_2, E_1, E_2, η_1, η_2 and n=11 for measurements of τ_3, E_3 and η_3. n indicates number of embryos.

Supplementary Note 1

Theoretical description of posterior body axis elongation. At supracellular length scales and developmental time scales, tissues can be physically described as continuum materials[23]. We simulate the physical expansion of a 2D dorsal-ventral projection of the presomitic mesoderm (PSM) and mesodermal progenitor zone (MPZ) tissues, with x and y defining the anteroposterior (AP) and mediolateral (ML) axes, respectively (Fig. S3 below). All our measurements indicate that the tissue transits from a fluid-like state in the MPZ to a solid-like state in the PSM. To simulate the observed fluid-to-solid jamming transition along the AP axis, we describe the tissue as a viscous fluid with inhomogenous viscosity along the AP axis, diverging as the tissue transits to a solid-like state (Fig. S3 below). The dynamics of the tissue is governed by two fundamental physical laws, namely momentum conservation (which reduces here to local force balance because inertial terms are negligible for embryonic tissues) and mass balance, which read

$$-\nabla p + \nabla \cdot \left(\mu(x) \left(\nabla \mathbf{u} + \nabla \mathbf{u}^{\mathrm{T}} \right) - \frac{2}{3} \mu(x) \left(\nabla \cdot \mathbf{u} \right) \mathbf{I} \right) = 0 \,, \tag{1}$$

$$\nabla \cdot \mathbf{u} = \frac{Q(x)}{\rho} \,, \tag{2}$$

where $\mathbf{I}$ is the identity tensor and p, $\mathbf{u}$ and ρ are the tissue pressure, velocity and density, respectively. Since our measurements indicate that the cell density in the tissue is uniform (see Extended Figure 9), we restricted the equations above to the case of uniform tissue density. The functions $\mu(x)$ and $Q(x)$ are the only inputs of the simulation and represent the spatial profile of the tissue viscosity along the AP axis and the spatial distribution of cell ingression rate from dorsal-medial (DM) tissues along the AP axis, respectively (Fig. S3 below). Ingression of cells to the MPZ from DM tissues occurs only within a region of size λ_Q from the extending posterior leading edge of the tissue[15]. This process can be accounted by the following functional form of Q:

$$Q(x) = \frac{Q_0}{1 + \exp\left(\dfrac{(x_{\mathrm{tip}} - \lambda_Q) - x}{a} \right)} \,, \tag{3}$$

where Q_0 is the maximal cell ingression rate, x_{tip} is the position of the extending posterior leading edge of the tissue (and changes as the tissue expands over time) and a is a length scale that defines how sharply the profile $Q(x)$ vanishes anteriorly. The inhomogenous viscosity along the AP axis is represented by the following functional form of the viscosity profile along the AP axis:

$$\mu(x) = \mu_{\mathrm{p}} + \frac{\mu_{\mathrm{a}} - \mu_{\mathrm{p}}}{1 + \exp\left(\dfrac{x - (x_{\mathrm{tip}} - \lambda_\mu)}{a} \right)} \,, \tag{4}$$

where μ_{p} and μ_{a} are the viscosities of the MPZ and PSM tissues, respectively. As explained above, the observed fluid-to-solid jamming transition is accounted for by a sharply diverging viscosity ($\mu_a \gg \mu_p$) as the tissue becomes solid-like at a distance λ_μ from the extending posterior leading edge of the tissue. In this case, the length scale a defines how sharply the viscosity diverges at the jamming transition. To simulate the expansion of the tissue in the absence of a fluid-to-solid transition, we simply consider the case of uniform viscosity, with the PSM viscosity being the same as that of the MPZ ($\mu_a = \mu_p$).

Finally, in order to completely determine the problem, it is necessary to specify the boundary conditions. In these simulations the tissue boundary is not imposed or fixed (free boundary problem), but rather the tissue shape is an outcome of the simulations, with the exception of the anterior-most boundary, which we anchor to a fixed wall (Fig. S3 below). At the boundary, local normal forces must balance and velocities must be continuous. Local normal force balance (equivalent to Laplace's Law) reads

$$\Delta p = \gamma \kappa \,, \tag{5}$$

where Δp is the pressure jump at the tissue boundary, γ is the tissue surface tension and κ is the curvature of the tissue surface (there is contribution from one principal curvature only because of the 2D nature of this simulation). For simplicity, we assume the tissue surface tension to be uniform along the AP axis. Finally, the viscosity of the fluid exterior to the tissue is negligible compared to the viscosity of the tissue anywhere along the AP axis.

The system is characterized by three dimensionless parameters that control the different possible behaviors. First, the ratio of the characteristic length scales λ_μ/λ_Q. Previous observations indicate that cell ingression in the MPZ from DM tissues occurs mostly at the posterior half of the MPZ tissue[15], indicating that $\lambda_\mu \gtrsim \lambda_Q$. For this reason, we simulated the system for $\lambda_\mu \simeq 2\lambda_Q$. Second, the ratio of surface stresses associated with tissue surface tension and shear stresses associated to tissue flows. In order to obtain any tissue shape different than a growing spherical blob, the shear stresses need to be similar or larger than the stresses associated to the tissue surface tension. For this reason, we simulated the system when the scale of shear stresses is similar than the scale of stresses associated to tissue surface tension. Third, the ratio of the PSM and MPZ viscosities, namely μ_a/μ_p. As explained above, this ratio is very large ($\mu_a \gg \mu_p$) in the presence of a fluid-to-solid jamming transition, since the PSM tissue becomes solid-like. For this reason, when simulating the system in the presence of a jamming transition, we choose $\mu_a \simeq 10^3\,\mu_p$, which effectively accounts for the divergence of the viscosity in the solid-like PSM from a numerical perspective. When studying the effects on morphogenesis of the absence of the jamming transition, we impose a uniform tissue viscosity ($\mu_a = \mu_p$), while keeping all other parameters the same.

We use COMSOL Multiphysics 5.3 to perform a Finite Element simulations of the system described above. We initialize the simulation with a tissue shaped as a semi-circle (initial condition for the tissue shape) in a box of fluid with negligible viscosity compared to the tissue (such as water). The simulation box is made much larger than the tissue size (by at least a factor of 10) to avoid any undesired boundary effects. The two ends of the semi-circle in contact with the fixed wall ($x = 0$) are anchored, and no tissue flow is allowed through the fixed wall. For a given simulation, the viscosity profile along the AP axis (Eq. 4) and the spatial profile of cells ingressing to the MPZ from DM tissues (Eq. 3) are provided as inputs to the simulation (Fig. S3 below). Once the initial system is set, we define an adaptive finite element mesh in COMSOL that is thereafter dynamically refined as the shape evolves to properly resolve fine features in the tissue shape and morphogenetic flows (Fig. S3c below). The simulations predict the shape of the extending tissue (boundary; Fig. 1b below) and morphogenetic flows (velocity field; inset in Fig. 4d, main text) that result from the given inputs according to fundamental physical laws (force and mass balance).

To understand the shape and dynamics of the tissue in the presence of the observed fluid-to-solid jamming transition, we performed simulations for $\mu_a \gg \mu_p$ which numerically encodes a transition from fluid-like to solid-like tissue states at a length λ_μ from the extending posterior leading edge of the tissue (Fig. 4c,d in the main text). In these conditions, the tissue extends unidirectionally and posteriorly (Fig. 4c,d in the main text), as observed experimentally. The

predicted tissue morphogenetic flows in the presence of the reported jamming transition display high posterior-directed velocities at the posterior end, no tissue flow in the A-PSM, and the existence of two counter-rotating vortices as the tissue transits from fluid-like to solid-like states (inset in Fig. 4d, main text).

To understand the shape and dynamics of the tissue in the absence of the observed fluid-to-solid jamming transition, we simulate the system with exactly the same $Q(x)$ profile, but with uniform tissue viscosity along the AP axis. In this case, the tissue expands isotropically, like a growing spherical blob, but does not display unidirectional elongation (Fig. 4e in the main text).

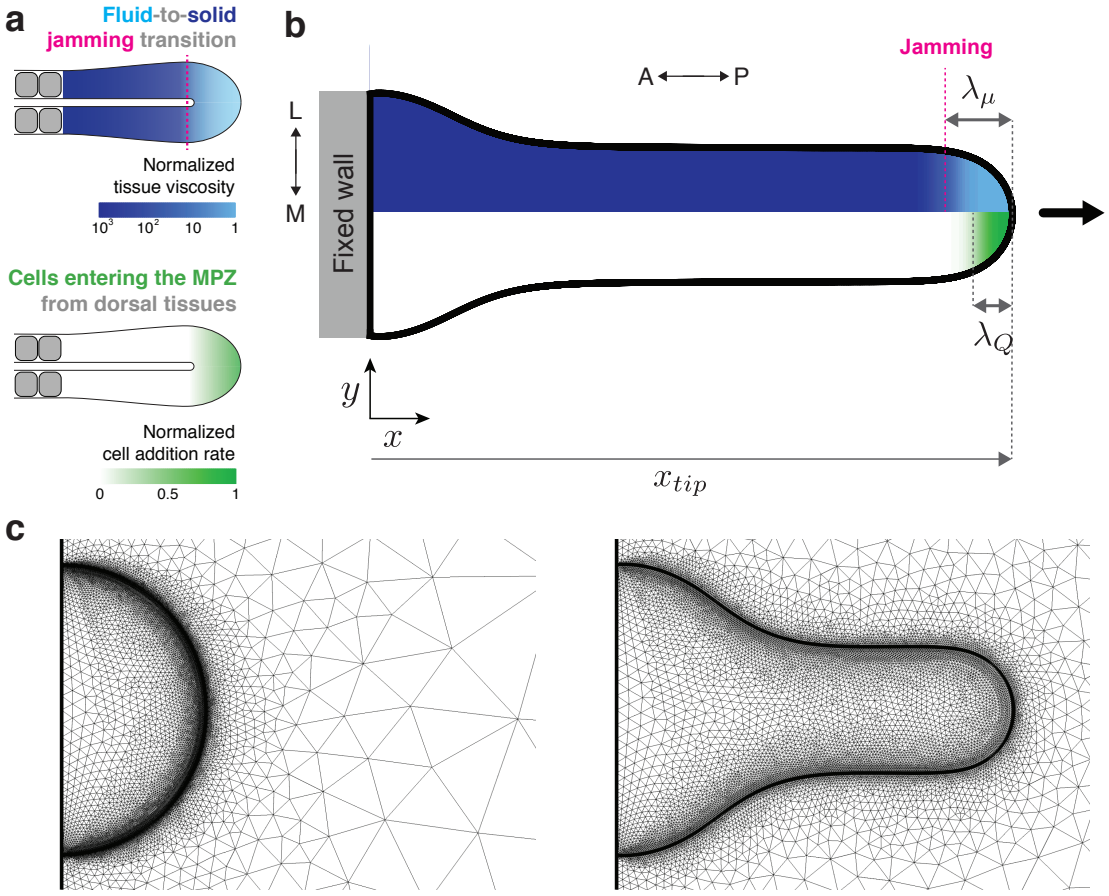

Figure S3: **Main elements of the simulation.** **a**, Sketch of posterior body elongation depicting the input to the simulations: jamming transition (light blue fluid-like tissue; violet solid-like tissue) and cell ingression into the MPZ from DM tissues (shades of green). **b**, Snapshot of a simulated elongating tissue showing the spatial profiles of tissue viscosity, $\mu(x)$, and cell ingression rate, $Q(x)$, along the AP axis, respectively. The fluid-to-solid jamming transition is simulated by a sharp increase in the tissue viscosity (magenta dashed line), with a very large viscosity simulating the solid tissue state. The color code in the top half of the shape corresponds to the spatial profile of the tissue viscosity, whereas the bottom half shows the AP profile of cell ingression rate into the MPZ from DM tissues. The gray rectangle at the anterior end (x=0) represents a fixed wall. The location $x_{\rm tip}$ corresponding to the position of the extending posterior leading edge of the tissue, and both λ_μ and λ_Q, are also shown. **c**, Snapshots of the finite element mesh for the initial tissue shape (semi-circle; left) and of the refined mesh after the simulations have evolved the tissue shape over time (right).